Available online at www.sciencedirect.com
SCIENCE DIRECT®
Physics Letters B 595 (2004) 60–67
PHYSICS LETTERS B
www.elsevier.com/locate/physletb

Aperture method to determine the density and geometry of antiparticle plasmas

ATRAP Collaboration

P. Oxley [a], N.S. Bowden [a], R. Parrott [a], A. Speck [a], C.H. Storry [a], J.N. Tan [a], M. Wessels [a], G. Gabrielse [a,1], D. Grzonka [b], W. Oelert [b], G. Schepers [b], T. Sefzick [b], J. Walz [c], H. Pittner [c], T.W. Hänsch [c,d], E.A. Hessels [e]

[a] *Department of Physics, Harvard University, Cambridge, MA 02138, USA*
[b] *IKP, Forschungszentrum Jülich GmbH, 52425 Jülich, Germany*
[c] *Max-Planck-Institut für Quantenoptik, Hans-Kopfermann-Strasse 1, 85748 Garching, Germany*
[d] *Ludwig-Maximilians-Universität München, Schellingstrasse 4/III, 80799 München, Germany*
[e] *Department of Physics and Astronomy, York University, Toronto, Ontario M3J 1P3, Canada*

Received 16 April 2004; received in revised form 28 April 2004; accepted 30 April 2004

Available online 23 June 2004

Editor: L. Rolandi

Abstract

The density and geometry of $\bar{p}$ and e^+ plasmas in realistic trapping potentials are required if the rate of antihydrogen formation from them is to be understood. A new measurement technique determines these properties of trapped positron (e^+) and antiproton ($\bar{p}$) plasmas, the latter for the first time. The method does not require the common assumption of a spheroidal plasma geometry, which only pertains for a perfect electrostatic quadrupole trapping potential. Plasma densities, diameters, aspect ratios and angular momenta are deduced by comparing the number of particles that survive transmission through an aperture, to that obtained from self-consistent solutions of Poisson's equation. For $\bar{p}$ the results differ substantially from the spheroid plasmas of an ideal Penning trap. The angular momentum of the plasma emerges as smooth function of the number of particles in the plasma, independent of the depth of the potential well that confines them.

PACS: 36.10.-k

Slow antihydrogen ($\bar{H}$) has so far been produced as positrons (e^+) cool antiprotons ($\bar{p}$) [1] to the low relative velocity needed for $\bar{H}$ formation within a nested Penning trap [2]. The production of slow $\bar{H}$ by this method was confirmed by two different detection mechanisms—by counting $\bar{p}$ and e^+ annihilations that are within 5 μs and ±8 mm of each other [3] and by field ionizing the $\bar{H}$ [4,5] for background-free detection.

The geometry and densities of the single component plasmas of e^+ and $\bar{p}$ are needed as a first step to understanding the $\bar{H}$ formation rate. These proper-

E-mail address: gabrielse@physics.harvard.edu (G. Gabrielse).
[1] ATRAP Spokesperson.

0370-2693/$ – see front matter
doi:10.1016/j.physletb.2004.04.084

ties have never been measured for a $\bar{p}$ plasma. Imaging trapped $\bar{p}$ annihilations on background gas has yielded only a very coarse resolution, nearly the size of our trap radius [6]. Positron plasmas have been characterized by several methods, but these have limitations in our context. The simplest method would be to eject the trapped plasmas along magnetic field lines to position sensitive detectors [7], but such detectors would block $\bar{p}$ and e^+ entry into the 4.2 K trap from opposite ends. A useful e^+ characterization method is to compare the frequency of a hydrodynamic mode of the plasma to what has been calculated [8,9]. This has been done successfully in the limit of thin drumhead plasma shapes [10] and in the limit of extremely large numbers of e^+ [11,12]—neither of which pertain to our experiments so far. For the large numbers of e^+, spheroidal plasma shapes were assumed, even though these apply only when there is a perfect, electrostatic quadrupole trapping potential. The potentials within the open access cylindrical Penning trap designs [13] used for $\bar{H}$ production [3–5] are not a good approximation to a quadrupole near the trap electrodes.

In this Letter, we deduce the plasma density, diameter, aspect ratio, and angular momentum of trapped $\bar{p}$ and e^+ plasmas by a new method. No assumption of a spheroidal plasma shape is needed owing to the use of a self-consistent solution to Poisson's equation [14]. The method does not require huge plasmas, and e^+ and $\bar{p}$ access from the ends of the trap is not obstructed. This first measurement of the geometry of a $\bar{p}$ plasma reveals a $\bar{p}$ plasma that is far from spheroidal. Just as striking, we observe e^+ plasmas that are surprisingly spheroidal even when they extend into regions where there are large departures from an ideal electrostatic quadrupole potential. The angular momentum for e^+ plasmas is shown to increase smoothly with e^+ number, independent of the depth of the confining potential well.

The density and geometry of the e^+ and $\bar{p}$ plasmas depend, of course, on how these particles are accumulated into the trap. In the examples used to illustrate the method, e^+ in a 3 mm diameter beam slow in a thin moderator crystal, pick up an electron as they exit this crystal, and are trapped when the electric field of a trap is able to remove this electron [15]. The $\bar{p}$ plasmas are accumulated (or stacked) [16,17] from pulses of 5 MeV $\bar{p}$ from CERN's AD that slow as they pass through thin vacuum windows, a PPAC detector, a gas moderator cell, and finally a Be degrader window. A preloaded plasma of cold electrons (loaded using a field emission point for most of the illustrations used here) cools the $\bar{p}$; its diameter determines the geometry of the cooled $\bar{p}$ which are measured.

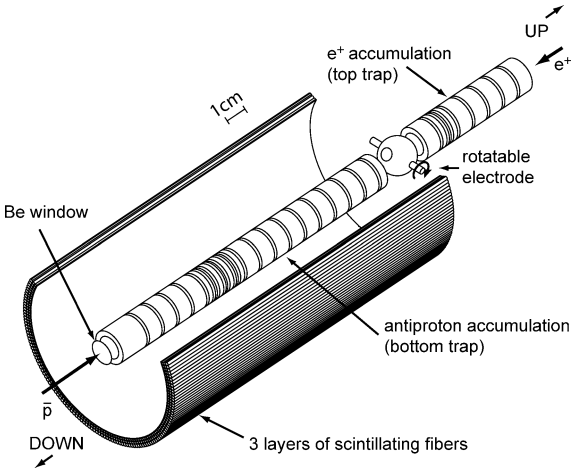

Fig. 1. Overview of the trap and fiber detector. Antiprotons are accumulated in the lower region (left), below the rotatable electrode aperture, while e^+ are accumulated in the upper region (right).

Penning traps for confining e^+ and $\bar{p}$ are formed by biasing a stack of 32 cylindrical electrodes (Fig. 1) that are aligned with a $B = 5.4$ T magnetic field, as has been described [1]. Antiprotons from CERN's AD facility are loaded into one end of the trap structure [17], while e^+ from a ^{22}Na source are loaded into the other via a method that involves the ionization of Rydberg positronium [15]. The electrodes are within a vacuum enclosure kept at 4.2 K via thermal contact with liquid helium; the pressure within a similar apparatus was measured to be better than 5×10^{-17} Torr [18].

To count $\bar{p}$ we release them from the trap by reducing the trapping potential, and count the coincidence signals produced by annihilation pions passing through surrounding scintillating fibers (Fig. 1) and large scintillator paddles farther from the trap. The well calibrated detection efficiency is about 50% and there is negligible background. Trapped e^+ are counted nondestructively using familiar radio-frequency techniques [19].

The aperture method of determining the density and geometry of trapped plasmas involves several steps. Plasmas stored in the 12 mm diameter electrodes in

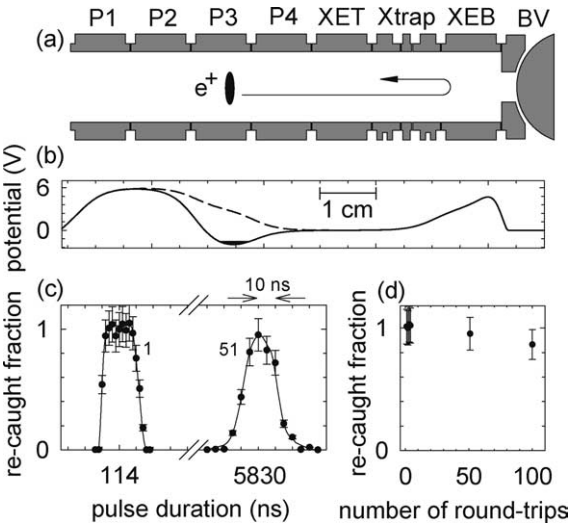

Fig. 2. Electrodes (a) and potentials (b) used to launch and recapture e^+. The recapture efficiency is high for 1 and 51 round trips (c) and decreases slightly as a function of the number of round trips (d).

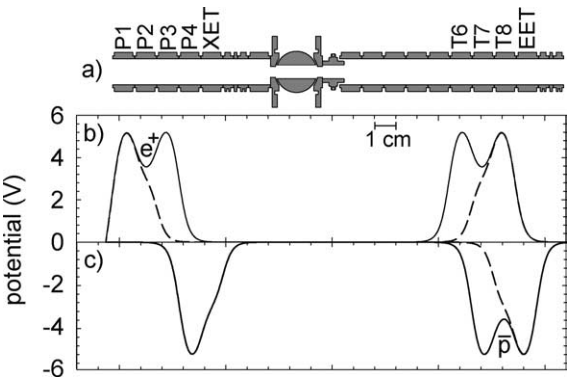

Fig. 3. Electrodes (a) and potentials used to pulse e^+ (b) and $\bar{p}$ (c) through the aperture. During a pulse the potential changes from the solid to the dashed curves.

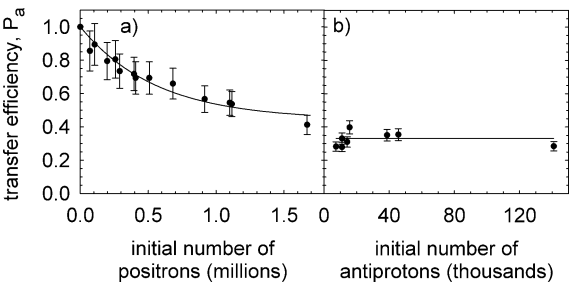

Fig. 4. Efficiency at which e^+ (a) and $\bar{p}$ (b) plasmas make one pass through the aperture as a function of the number of particles in the plasma.

the accumulation regions of the trap are analyzed by passing them through an aperture with a diameter $2a = 5$ mm that is presented when the rotatable electrode is in its open position, and then recapturing them. The number of particles in the plasma is counted (using techniques mentioned above) before and after it travels through the aperture to determine the transmitted fraction P_a. This is then compared to the efficiency that is calculated for various particle geometries to determine which of these plasma configurations we have, as will be described.

Fig. 2 illustrates that we can apply the fast voltage pulses required to launch and then recapture e^+ with near unit efficiency for a round trip (Fig. 2(c)) that is not through the aperture. The efficiency remains nearly this high after 100 round trips (Fig. 2(d)). Much less precise timing is required for $\bar{p}$ than for e^+ owing to the larger $\bar{p}$ mass. The considerable challenge is that most devices able to change the potential in less than 10 ns, as required by e^+ transit times, introduce noise that heats up the trapped particles, often driving them from the trap. We used programmable pulse generators driving saturated FET switches which produce 20 V pulses with a rise time of 3 ns. Attenuators can reduce the amplitude, and toroid transformers can invert the voltage sign of electrical pulses sent through 1.5 m of stainless-steel microcoax cable, to matching networks near the trap that reduce reflections. Up to 8.5 V pulses can be applied to the electrodes, with rise times less than 4 ns and relative timing precision better than 1 ns. Changing from the solid to dashed potential in Fig. 2(b) requires changing the potential on electrode P3 from -3 to 3 V.

Similar switched potentials are used to launch e^+ (Fig. 3(b)) and $\bar{p}$ (Fig. 3(c)) from one side of the aperture and catch them on the other. The e^+ are in wells that are 0.8, 1.6 and 2.3 V deep on axis, and the $\bar{p}$ are in a 1.6 V well. Fig. 4 shows the measured transfer efficiency P_a for e^+ and $\bar{p}$ sent through the aperture as a function of the number of particles in the respective plasmas. For e^+, the transfer efficiency decreases from near unity as the number increases and the plasma size grows. In marked contrast, the $\bar{p}$ plasma always has a large diameter, even for small numbers of $\bar{p}$, so that

a large fraction of the $\bar{p}$ do not make it through the aperture. We discuss possible reasons presently.

To make these measurements, the e^+ are counted nondestructively before and after a trip through the aperture, using electronics connected to the electrodes of harmonic traps on both sides of the aperture. The $\bar{p}$ are counted by ejecting them from the trap and using the efficient annihilation detectors mentioned above. Two identically prepared $\bar{p}$ plasmas are used; one is simply ejected from the trap to get a normalization signal. The second is sent through the aperture and bounced back to ensure that the counted annihilations take place in the same location as those from the normalization plasma. Varying the number of passes through the aperture establishes the small ($\sim 10\%$) correction needed to account for losses on the additional pass through the aperture.

What remains is to relate the measured transmission efficiency P_a through an aperture of radius a, to the properties of a plasma comprised of N particles of charge q and mass m. The plasma is confined by a magnetic field B (equivalently specified by its cyclotron frequency $\omega_c = qB/m$) and an electrostatic potential well. The cylindrical symmetry makes it natural to use cylindrical coordinates ρ and z.

For the familiar special case of a perfect electrostatic quadrupole trapping potential, a single component plasma assumes a spheroidal shape (Fig. 5) with a density that is uniform out to a boundary that drops off abruptly in a Debye screening length. Here a "spheroid" is an ellipsoid with rotational symmetry about the magnetic field direction $\hat{\mathbf{z}}$. The strength of the potential well is indicated by the angular frequency ω_z of the plasma's center-of-mass oscillation along the magnetic field direction. In this idealized case, the plasma is a spheroid of maximum radius ρ_p and maximum axial half-length $\alpha\rho_p$ (i.e., with aspect ratio α).

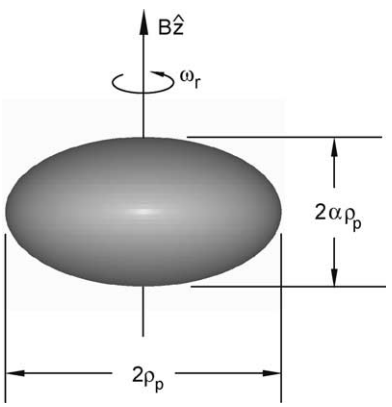

Fig. 5. Ideal, spheroidal plasma.

We seek to determine the three crucial parameters of the ideal spheroidal plasma—its radius ρ_p and aspect ratio α, along with its uniform density n, equivalently specified by the angular plasma frequency $\omega_p^2 = e^2 n/(\epsilon_0 m)$. Of the three independent relations that must be solved to get the three parameters, the first two are familiar properties of a spheroidal plasma [9]:

$$N = \frac{4\pi}{3}\alpha\rho_p^3 n, \tag{1}$$

$$\left(\frac{\omega_z}{\omega_p}\right)^2 = \frac{1}{\alpha^2-1}Q_1^0\left(\frac{\alpha}{\sqrt{\alpha^2-1}}\right)$$

$$\text{with} \quad Q_1^0(z) \equiv \frac{z}{2}\ln\left(\frac{z+1}{z-1}\right) - 1. \tag{2}$$

The aperture adds a third equation relating P_a to ρ_p; P_a is just the fraction of the spheroidal plasma that is within $\rho_p < a$.

$$P_a = 1 - \left[1 - \left(\frac{a}{\rho_p}\right)^2\right]^{3/2}. \tag{3}$$

The third equation determines ρ_p when $\rho_p > a$. When this condition is not met, for small numbers of trapped particles, then $P_a = 1$ instead and we do not have enough equations to solve for the three unknowns. The three equations and thus their solutions depend upon the measured values N, P_a, ω_c and ω_z.

The spheroidal plasma characterized by n, ρ_p and α (Fig. 5) rotates rigidly at angular frequency ω_r about $\hat{\mathbf{z}}$

$$\omega_r = \frac{\omega_c}{2}\left[1 - \sqrt{1 - 2\left(\frac{\omega_p}{\omega_c}\right)^2}\right] \approx \frac{\omega_p^2}{2\omega_c}, \tag{4}$$

with the (very good) approximation applying when $\omega_c \gg \omega_p$ as it is here.

When the trapping potential is not a perfect electrostatic quadrupole potential, the plasma shape need not be spheroidal. The potential within a real trap is never perfect, especially within simple uncompensated traps, and it is typically far from the ideal quadrupole near the electrodes of the trap. An attractive feature of the aperture method is that there is no need to assume a spheroidal plasma shape. A self-consistent solution

to Poisson's equation,

$$\nabla^2\phi(\rho,z) = -qn(\rho,z)/\epsilon_0, \tag{5}$$

determines the combined potential $\phi(\rho,z)$ of the trap and the particle charge density $n(\rho,z)$ in a mean field approximation. We use a code that is adapted slightly from what was generously provided to us by Spencer [14] to calculate the possible geometries of an N particle plasma in global thermal equilibrium, labeling each possible configuration by its largest radial extent, ρ_p. The minor adaptations allow us to input fixed N and ρ_p instead of fixed central density $n(0,0)$ and ρ_p. In global thermal equilibrium a plasma rotates at a single rotation frequency ω_r which is effectively an average over the thermal fluctuations of individual particles.

We assume that both e^+ and $\bar{p}$ are in thermal equilibrium at temperature $T = 4.2$ K. This is a very good assumption for the e^+ since, like the cooling electrons, these cool to the 4.2 K temperature of their surroundings by radiating synchrotron radiation. The $\bar{p}$ situation is more complicated. They are initially cooled by collisions with 4.2 K electrons to the same temperature. We assume that they keep this temperature, and the results to be described are in fact not very sensitive to variations in the temperature used. Moreover, the observed time for axial energy redistributions via $\bar{p}$–$\bar{p}$ collisions is of order ten seconds [4], shorter than the minute or so available for the $\bar{p}$ to equilibrate. The radial equilibration time for the $\bar{p}$ is less clear. Long range collisions seemed to be responsible for radial equilibration of Mg^+ ions [20]. The time required for radial equilibration seems comparable to the time available when scaled to our conditions.

For a given N, ρ_p and T, the self-consistent solutions determine the possible densities $n(\rho,z)$ and shapes for the plasma, and the angular frequencies at which it rotates, ω_r. (For small ρ_p—plasmas that are near the central axis and far away from the trap electrodes—we recover the spheroids that pertain for an ideal quadrupole potential.) For each configuration (i.e., for each ρ_p) we calculate the transmission efficiency P_a by integrating $n(\rho,z)$ over the volume $\rho < a$. The measured transmission efficiency P_a then indicates which of the possible configurations is present in our trap, thereby determining the density profile $n(\rho,z)$ and the rotation frequency ω_r. Also determined is the total angular momentum

$$\begin{aligned} L_z &= m\omega_r \sum_{i=1}^{N} \rho_i^2 + \frac{1}{2} m\omega_c \sum_{i=1}^{N} \rho_i^2 \\ &\approx \frac{1}{2} m\omega_c N \rho_{\mathrm{rms}}^2. \end{aligned} \tag{6}$$

The first, mechanical term is so much smaller than the second, field term that the approximation to the right applies, with $\rho_{\mathrm{rms}}^2 \equiv \sum_{i=1}^{N} \rho_i^2/N$.

The e^+ plasma parameters are plotted in Fig. 6 as a function of the number of positrons, for plasmas in the three mentioned potential wells. The central density $n(0,0)$, diameter, axial extent, and aspect ratio all grow slowly with increasing number of e^+. The angular momentum, presumably a property of the loading process, does not change with the depth of the potential well, owing to the cylindrical symmetry. For small numbers of e^+ we have thin "pancake" clouds ($\alpha \to 0$). In this limit, Fig. 6(e) shows that the rotation frequency ω_r approaches the single particle magnetron frequency $\omega_z^2/(2\omega_c)$, as expected. A $\pm 10\%$ uncertainty in the N is reflected in the error bars.

The diameter of the thin, pancake shaped $\bar{p}$ plasma changes very little as the number N of $\bar{p}$ is increased (Fig. 7), while the axial extent, and hence the aspect ratio α, grow linearly with N. The error bars represent a $\pm 10\%$ uncertainly in N. If we had assumed idealized spheroidal plasma shapes we would mistakenly have concluded that the $\bar{p}$ parameters were changing as the dashed lines. The density that increases with N is the average density of the plasma, since this provides the most realistic measure of the density of the whole $\bar{p}$ cloud. The central density of thin clouds is appreciably lower than the average due to the thermal energy of the particles and the deviation from a quadrupole trapping potential [21,22].

A relatively small number of $\bar{p}$ and only one potential well, 1.6 V deep on axis, are used as examples because $\bar{p}$ accumulation takes a long time. Now that the usefulness of the method is demonstrated it can be applied to plasmas that are accumulated differently than our example plasmas—for example, to the much larger number of $\bar{p}$ used for slow $\bar{H}$ experiments (open circles in Fig. 7). These $\bar{p}$ were cooled and accumulated using cooling electrons loaded when fast e^+ from a radioac-

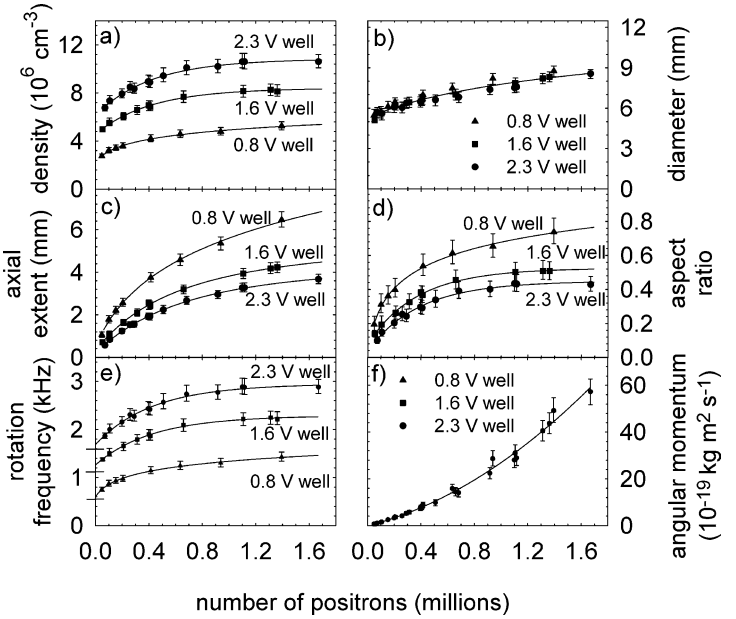

Fig. 6. (a)–(f) Parameters of e^+ plasmas in potential wells of three different depths. The density is $n(0,0)$. For low numbers of e^+, ω_r approaches the one-particle magnetron frequency $\omega_m = \omega_z^2/(2\omega_c)$ indicated by the segments crossing the left vertical axis of (e), as expected. The solid curves are to aid the eye.

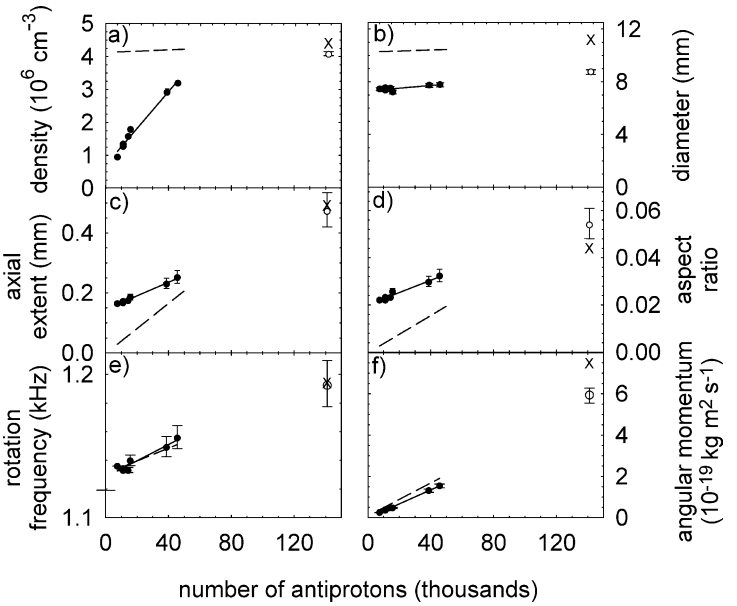

Fig. 7. Parameters of $\bar{p}$ plasmas in a well that is 1.6 V deep on axis. The dashed curves and the X points are what would have been mistakenly deduced if a spheroid plasma shape had been assumed. The density is the average of $n(\rho, z)$. For low numbers of $\bar{p}$, ω_r approaches the one-particle magnetron frequency $\omega_m = \omega_z^2/(2\omega_c)$ indicated by the segment crossing the left vertical axis of (e), as expected. The solid curves are to aid the eye.

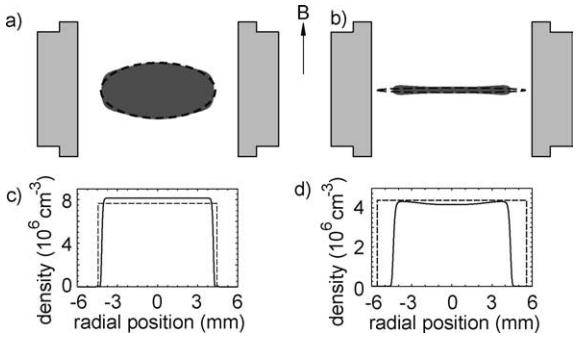

Fig. 8. Plasma boundaries for 1.4 $\times 10^6$ e^+ (a) and for 1.4 $\times$ 10^5 $\bar{p}$ (b), both within an electrode of the trap in Fig. 3(a). The spheroid approximation (dashes) is not good for the $\bar{p}$ but is much better for the e^+. Corresponding midplane density profiles are in (c) and (d).

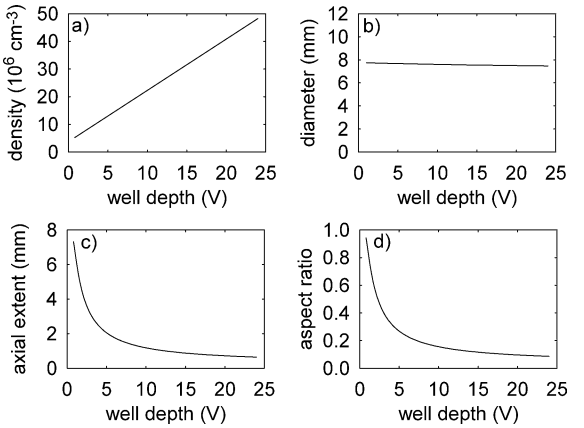

Fig. 9. Extrapolated density, diameter, axial extent and aspect ratio for 1 million e^+ in a potential well as a function of the potential well depth on axis.

tive source scattered off background gas atoms they liberated from cold trap surfaces.

For the larger e^+ and $\bar{p}$ plasmas used for $\bar{H}$ experiments the solid curves in Fig. 8 show typical e^+ (a) and $\bar{p}$ (b) plasma geometries. The $\bar{p}$ plasma boundary clearly differs from the (dashed) spheroid that would pertain for a perfect electrostatic potential (Fig. 8(b)). By contrast, the boundary of a typical e^+ plasma in Fig. 8(a) is well approximated by a spheroid except for small deviations near the electrodes, where the trap potential differs most from an ideal electrostatic quadrupole. The deviations are more visible in the midplane density profiles in Fig. 8(c) and (d).

One caution about the smaller $\bar{p}$ plasmas is that their axial extent falls slightly below the Debye length and becomes comparable to the inter-particle spacing. The self-consistent solution to Poisson's equation utilizes a mean field approach—not likely to be especially accurate for our smallest plasmas that are only a couple of particles thick, though such small $\bar{p}$ plasmas are not used for $\bar{H}$ experiments.

The fast pulsing electronics that is quiet enough to avoid serious heating of the plasmas permits us to apply the aperture method to well depths no deeper than 2.3 V on axis. To estimate the parameters of larger e^+ plasmas in deeper wells used in later $\bar{H}$ experiments the measured parameters in Fig. 6 can be extrapolated to potential wells of different depths. The angular momentum L_z is especially useful since Fig. 6 shows it to be independent of well depth. Fig. 9 shows an extrapolation for 10^6 e^+ in potential wells of increasing depth on axis. This must be checked, of course, when better electronics becomes available.

The density and geometry of trapped single component plasmas of e^+ and $\bar{p}$ have been measured by an aperture method—the first time that $\bar{p}$ plasmas have been characterized. The method does not require assuming a spheroidal plasma geometry which only pertains for a perfect electrostatic quadrupole trapping potential. The e^+ cloud shapes turn out to be approximately spheroidal. The $\bar{p}$ plasma shapes are definitely not. The measured transmission through a aperture together with self-consistent solutions of Poisson's equation show the $\bar{p}$ radial extent to be appreciably smaller than that for a plasma in ideal Penning trap fields. Applied to $\bar{H}$ formation, the $\bar{p}$ radius used by ATRAP is larger than the e^+ radius so that the $\bar{H}$ production rate would be enhanced with $\bar{p}$ plasmas of smaller radius. The aperture method makes it possible to determine the geometry of the $\bar{p}$ and e^+ plasmas, along with the density of the latter. These antimatter plasma properties are critical if there is to be quantitative understanding of $\bar{H}$ production rates.

Acknowledgements

We are grateful to CERN, its PS Division and the AD team for delivering antiprotons, to Ross Spencer for providing the computer code, and to J. Bollinger and R. Spencer for helpful comments. This work

was supported by the NSF, AFOSR, the ONR of the US, the BMBF, MPG and FZ-J of Germany, and the NSERC, CRC, CFI and OIT of Canada.

References

[1] G. Gabrielse, J. Estrada, J.N. Tan, P. Yesley, N.S. Bowden, P. Oxley, T. Roach, C.H. Storry, M. Wessels, J. Tan, D. Grzonka, W. Oelert, G. Schepers, T. Sefzick, W. Breunlich, M. Cargnelli, H. Fuhrmann, R. King, R. Ursin, H. Zmeskal, H. Kalinowsky, C. Wesdorp, J. Walz, K.S.E. Eikema, T. Hänsch, Phys. Lett. B 507 (2001) 1.
[2] G. Gabrielse, S.L. Rolston, L. Haarsma, W. Kells, Phys. Lett. A 129 (1988) 38.
[3] M. Amoretti, et al., Nature 419 (2002) 456.
[4] G. Gabrielse, N.S. Bowden, P. Oxley, A. Speck, C.H. Storry, J.N. Tan, M. Wessels, D. Grzonka, W. Oelert, G. Schepers, T. Sefzick, J. Walz, H. Pittner, T.W. Hänsch, E.A. Hessels, Phys. Rev. Lett. 89 (2002) 213401.
[5] G. Gabrielse, N.S. Bowden, P. Oxley, A. Speck, C.H. Storry, J.N. Tan, M. Wessels, D. Grzonka, W. Oelert, G. Schepers, T. Sefzick, J. Walz, H. Pittner, T.W. Hänsch, E.A. Hessels, Phys. Rev. Lett. 89 (2002) 233401.
[6] M.C. Fujiwara, et al., Phys. Rev. Lett. 92 (2004) 065005.
[7] J.H. Malmberg, C.F. Driscoll, Phys. Rev. Lett. 44 (1980) 654.
[8] D.H.E. Dubin, Phys. Rev. Lett. 66 (1991) 2076.
[9] J.J. Bollinger, D.J. Heinzen, F.L. Moore, W.M. Itano, D.J. Wineland, D.H.E. Dubin, Phys. Rev. A 48 (1993) 525.
[10] C.S. Weimer, J.J. Bollinger, F.L. Moore, D.J. Wineland, Phys. Rev. A 49 (1994) 3842.
[11] M.D. Tinkle, R.G. Greaves, C.M. Surko, R.L. Spencer, G.W. Mason, Phys. Rev. Lett. 40 (1994) 352.
[12] M. Amoretti, et al., Phys. Rev. Lett. 91 (2003) 55001.
[13] G. Gabrielse, L. Haarsma, S.L. Rolston, Int. J. Mass Spectrosc. Ion Phys. 88 (1989) 319;
G. Gabrielse, L. Haarsma, S.L. Rolston, Int. J. Mass Spectrosc. Ion Phys. 93 (1989) 121.
[14] R.L. Spencer, S.N. Rasband, R.R. Vanfleet, Phys. Fluids B 5 (1993) 4267.
[15] J. Estrada, T. Roach, J.N. Tan, P. Yesley, G. Gabrielse, Phys. Rev. Lett. 84 (2000) 859.
[16] G. Gabrielse, Adv. At. Mol. Opt. Phys. 45 (2001) 1.
[17] G. Gabrielse, N.S. Bowden, P. Oxley, A. Speck, C.H. Storry, J.N. Tan, M. Wessels, D. Grzonka, W. Oelert, G. Schepers, T. Sefzick, J. Walz, H. Pittner, E. Hessels, Phys. Lett. B 548 (2002) 140.
[18] G. Gabrielse, X. Fei, L.A. Orozco, R.L. Tjoelker, J. Haas, H. Kalinowsky, T.A. Trainor, W. Kells, Phys. Rev. Lett. 65 (1990) 1317.
[19] D.J. Wineland, H.G. Dehmelt, J. Appl. Phys. 46 (1975) 919.
[20] F. Anderegg, X.-P. Huang, C.F. Driscoll, E.M. Hollmann, T.M. O'Neil, D.H.E. Dubin, Phys. Rev. Lett. 78 (1997) 2128.
[21] G.W. Mason, R.L. Spencer, J.A. Bennett, Phys. Plasmas 3 (1996) 1502.
[22] D.L. Paulson, R.L. Spencer, Phys. Plasmas 5 (1998) 345.